 doi:10.20944/preprints202104.0180.v1

Article

Optical Intensity Far-Field Distribution of MEMS Micro-mirror Arrays by Fraunhofer Diffraction

Bin Zhang [1], Yu Zhang [1], Guohui Yang [2] and Chunhui Wang [1,3,*]

[1] National Key Laboratory of Tunable Laser Technology, Harbin Institute of Technology, Harbin, Heilongjiang, 150001, China; teamupl@yeah.net
[2] School of Electronic and Information Engineering, Harbin Institute of Technology, Harbin, Heilongjiang 150080, China; gh.yang@hit.edu.cn
[3] Glint Institute of AI and Robotics, Shenzhen, Guangdong, 518063, China;
* Correspondence: wangch_hitl@163.com; Tel.: (+86 13009802438)

Abstract: Compared with liquid crystal clad waveguide, MEMS mirror has some merits, such as higher-transmissivity, lager-angle of scanning, faster scanning speed and so on. Furthermore, MEMS mirror arrays perform more superior than MEMS mirror when they steer laser beam, which make MEMS arrays much more suitable to be used in devising compact Lidar. Before assembling a Lidar with MEMS arrays, the optical intensity and distributions of the laser diffracted by MEMS arrays should be analyzed, but few published papers about this issue are available so far, this paper will focus on this issue about MEMS arrays. Firstly, the complex amplitudes of laser which is diffracted by 1-D and 2-D arrays are presented, respectively. Then the optical intensity and distributions on the observation plane are presented. Finally, the simulation diagrams of these distributions are shown, and the correctness of the results is indirectly verified by Young's double-slit experiment. The results gotten in this letter are essential to design a compacted Lidar based on MEMS arrays.

Keywords: MEMS Mirror Arrays; Laser beam; Fraunhofer Diffraction; Optical Intensity

1. Introduction

In 1954, Charles Smith published an article which focused on silicon and germanium's stress-sensitive effects[1], Smith's research opened the prelude of semi-conductor industry. Sensor is a branch of research achievements of semi-conductor. Piezoresistive silicon pressure sensor and strain gauge were typical applications of quasi-MEMS (viz. Micro-electromechanical systems), which were born in 1960s[2]-[9]. Honeywell Research Center[2] and Bell Lab[2],[6] made great incipient contributions to this field. In the 1970s, the pressure sensor production signifies the birth of MEMS sensors[10]-[13]. In subsequent, with the micromachining improved and developed rapidly, inexpensive MEMS were massive production, which made MEMS widely used in automobile industry[14]-[17] and daily consumer electronics possible[18],[19].

MEMS micro-mirror and MEMS micro-mirror arrays were extensively applied in optics to date[20],[21], and they are indispensable in laser communication and imaging[22], especially in laser detection. MEMS micro-mirror has unique endowment when using it to design compact laser Lidar, but compared with MEMS micro-mirror, MEMS micro-mirror arrays perform much more excellent in the application field of large optical aperture, e.g. MEMS micro-mirror arrays can achieve a larger scanning angle in space laser communication system[23]. The majority of researches on MEMS micro-mirror arrays were majoring in adaptive light detection[24], and the mainstream of MEMS micro-mirror arrays is a chip composed of several mirrors[25], while Luo and his coworkers designed a circumferential-scan endoscopic by combining couples of MEMS micro-mirrors with C lenses[26].

Preprints (www.preprints.org) | NOT PEER-REVIEWED | Posted: 6 April 2021 doi:10.20944/preprints202104.0180.v1

The laser blueprints on the observation plane, which manipulated by MEMS mirror arrays, are much more meticulous than ones by single MEMS mirror. The difference between MEMS mirror with MEMS mirror arrays to manipulate laser is the former steers laser to scan a target through the mechanical vibration of mirror and the latter do it through a combination of light interference and mirrors vibration. So comparing with a Lidar based on single MEMS, the resolution and the imaging speed of a Lidar would be significantly increased which is based on MEMS arrays. But the prerequisites of devising a Lidar based on MEMS arrays are the analysis of optical intensity and distribution on the observation plane when the laser is diffracted by the arrays, they are seldom-reported so far. In this paper, we would solve this issue. On the basis of Kirchhoff and Fraunhofer diffraction theory, we calculate the optical intensity distribution in far-field from the arrays when the laser is diffracted by 1-D and 2-D MEMS micro-mirror arrays, and show some simulation diagrams to certify the results in the end.

2. Intensity Distribution Diffracted by 1-D MEMS Arrays

With Fraunhofer diffraction condition, as shown in Eq. (1), the Fraunhofer diffraction theory is an approximation of Kirchhoff diffraction theory in far-field, in other words, the Kirchhoff diffraction formula and the Fraunhofer diffraction equation become the same. Setting the reference as Fig.1, the Fraunhofer diffraction condition is

$$k\frac{(x_1^2+y_1^2)}{2z_1} << \pi, \tag{1}$$

where $k=\omega/c$ is the number of waves per second, ω and c are the angle frequency and the speed of laser, respectively, z_1 is the distance between the aperture of M with the plane of xP_0y. Supposing the electric component of incident laser beam is $\tilde{E}(X)e^{-i\omega t}$, if the coordinates of P_1 satisfy Fraunhofer diffraction condition, and the beam is diffracted by the aperture M, with Fraunhofer diffraction theory, the complex amplitude of point $P_1(x_1,y_1)$ is known as

$$\tilde{E}(x,y)=-\frac{ie^{ikz_1}}{\lambda z_1}e^{ik\frac{x^2+y^2}{2z_1}}\iint_M \tilde{E}(x_1,y_1)e^{-ik\frac{xx_1+yy_1}{z_1}}dx_1dy_1. \tag{2}$$

Taking the parameter of aperture M, whose sizes is $2a\times 2b$, into Eq. (2), there is

$$\tilde{E}(x,y)=-\frac{ie^{ikz_1}}{\lambda z_1}e^{ik\frac{x^2+y^2}{2z_1}}\int_{-a}^{a}\int_{-b}^{b}\tilde{E}(x_1,y_1)e^{-ik\frac{xx_1+yy_1}{z_1}}dx_1dy_1. \tag{3}$$

We take the beam as coherent light, so $\tilde{E}(x_1,y_1)$ equals a constant, and let it equal A, then integrating formula (3), it becomes the equation of

$$\tilde{E}(x,y)=-\frac{ie^{ikz_1}}{\lambda z_1}e^{ik\frac{x^2+y^2}{2z_1}}\left[A\frac{z_1^2}{k^2xy}4\sin\frac{ka}{z_1}x\sin\frac{kb}{z_1}y\right]. \tag{4}$$

For Eq. (3), when $x=0, y=0$, we get the complex amplitude at point $P_0(0,0)$, which is

$$\tilde{E}(P_0)=-A\frac{i}{\lambda z_1}e^{ik\left(z_1+\frac{x^2+y^2}{2z_1}\right)}2a\cdot 2b, \tag{5}$$

by combining Eq. (5) with Eq. (4), we obtain

Preprints (www.preprints.org) | NOT PEER-REVIEWED | Posted: 6 April 2021 doi:10.20944/preprints202104.0180.v1

$$\tilde{E}(x,y)=\tilde{E}_0\left(\frac{z_1}{kax}\sin\frac{ka}{z_1}x\right)\left(\frac{z_1}{kay}\sin\frac{kb}{z_1}y\right), \tag{6}$$

where $\tilde{E}_0=\tilde{E}(P_0)$, and if $\alpha=\frac{kax}{z_1}$, $\beta=\frac{kby}{z_1}$, then taking α and β into Eq. (6), there is

$$\tilde{E}(x,y)=\tilde{E}_0\frac{\sin\alpha}{\alpha}\frac{\sin\beta}{\beta}. \tag{7}$$

If the mirror is a square with side length $2a$, just substituting a for b of Eqs. (5-7) would be the accordingly results.

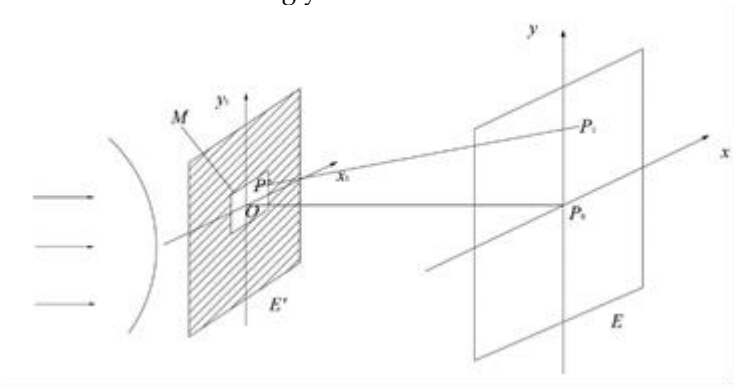

Figure 1. Fraunhofer diffraction schematic.

MEMS arrays can be divided into 2 categories, namely 1-D and 2-D as shown in Fig. 2. For generality of calculation, supposing 1-D arrays is composed of N pieces of $2a\times 2b$ mirrors, and the pitch between two consecutive mirrors is d. Fig. 3 is diffraction diagram by 1-D MEMS micro-mirror arrays. We set the coordinate system as Fig. 3, then the complex amplitude of laser on xP_0y plane is

$$\tilde{E}(x,y)=-\frac{\mathrm{i}e^{\mathrm{i}kz_1}}{\lambda z_1}e^{\mathrm{i}k\frac{x^2+y^2}{2z_1}}A\sum_{j=0}^{N-1}\int_{j(2a+d)-a}^{j(2a+d)+a}\int_{-b}^{b}e^{-\mathrm{i}k\frac{xx_1+yy_1}{z_1}}dx_1dy_1, \tag{8}$$

integrating Eq. (8), it renders

$$\begin{aligned}\tilde{E}(x,y)=&-\frac{\mathrm{i}A}{\lambda z_1}e^{\mathrm{i}kz_1+\mathrm{i}k\frac{x^2+y^2}{2z_1}}\left[-\frac{z_1}{\mathrm{i}ky}\left(e^{-\frac{\mathrm{i}ky}{z_1}b}-e^{\frac{\mathrm{i}ky}{z_1}b}\right)\right]\left[-\frac{z_1}{\mathrm{i}kx}e^{-\mathrm{i}k\frac{xx_1}{z_1}}\Big|_{-a}^{a}\right.\\&\left.+\left(e^{-\frac{\mathrm{i}kx}{z_1}(2a+d)}\right)\left(-\frac{z_1}{\mathrm{i}kx}e^{-\mathrm{i}k\frac{xx_1}{z_1}}\Big|_{-a}^{a}\right)+\ldots+\left(e^{-\frac{\mathrm{i}kx}{z_1}(N-1)(2a+d)}\right)\left(-\frac{z_1}{\mathrm{i}kx}e^{-\mathrm{i}k\frac{xx_1}{z_1}}\Big|_{-a}^{a}\right)\right]\\=&-\frac{\mathrm{i}Aab}{\lambda z_1}e^{\mathrm{i}kz_1+\mathrm{i}k\frac{x^2+y^2}{2z_1}}\frac{\sin\beta}{\beta}\left[1+e^{-\frac{\mathrm{i}kx}{z_1}(2a+d)}+\ldots+e^{-\frac{\mathrm{i}kx}{z_1}(N-1)(2a+d)}\right]\frac{\sin\alpha}{\alpha}\\=&-\frac{4\mathrm{i}Aab}{\lambda z_1}e^{\mathrm{i}kz_1+\mathrm{i}k\frac{x^2+y^2}{2z_1}}\frac{\sin\beta}{\beta}\frac{\sin\alpha}{\alpha}\left[\frac{1-e^{-N\frac{\mathrm{i}kx}{z_1}(2a+d)}}{1-e^{-\frac{\mathrm{i}kx}{z_1}(2a+d)}}\right].\end{aligned} \tag{9}$$

Preprints (www.preprints.org) | NOT PEER-REVIEWED | Posted: 6 April 2021 doi:10.20944/preprints202104.0180.v1

Where

$$\frac{1-e^{-N\frac{ikx}{z_1}(2a+d)}}{1-e^{-\frac{ikx}{z_1}(2a+d)}}=e^{\frac{-i(N-1)kx(2a+d)}{2z_1}}\frac{e^{\frac{iNkx(2a+d)}{2z_1}}-e^{-\frac{iNkx(2a+d)}{2z_1}}}{e^{\frac{ikx}{2z_1}(2a+d)}-e^{-\frac{ikx}{2z_1}(2a+d)}}$$
$$=e^{\frac{-i(N-1)kx(2a+d)}{2z_1}}\frac{\sin\left[Nkx(2a+d)/2z_1\right]}{\sin\left[kx(2a+d)/2z_1\right]}. \tag{10}$$

And if $C=-\frac{iA}{\lambda z_1}e^{ikz_1+ik\frac{x^2+y^2}{2z_1}}$ and $\Delta_x=kx(2a+d)/z_1$, combining Eq. (9) with Eq. (10), we obtain

$$\tilde{E}(x,y)=4Cabe^{-i(N-1)\frac{\Delta_x}{2}}\frac{\sin\beta}{\beta}\frac{\sin\alpha}{\alpha}\frac{\sin(N\Delta_x/2)}{\sin(\Delta_x/2)}. \tag{11}$$

By virtue of Eq. (11), the optical intensity at point $P(x,y)$ is gotten,

$$I(x,y)=\left|\tilde{E}(x,y)\right|^2=\left|4Cab\right|^2\left(\frac{\sin\beta}{\beta}\right)^2\left(\frac{\sin\alpha}{\alpha}\right)^2\left(\frac{\sin(N\Delta_x/2)}{\sin(\Delta_x/2)}\right)^2. \tag{12}$$

Then we can analyze the distribution characteristics of optical intensity in the plane of xP_0y based on Eqs. (11) and (12). On xP_0y plane, when the coordinates of one point equal the roots of Eq. (12), the brightness of the point would be the minimum. While getting the stripes of maximum brightness by analysis methods, we should take advantage of the derivative of Eq. (12), but this is rather challenging. In order to illustrate the contrast and resolution of the maximum stripes on the observation plane, we would show the simulation diagram of Eq. (12) in section 4.

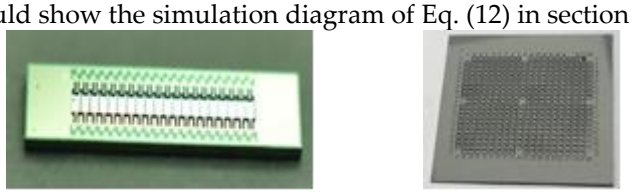

(**a**) (**b**)

Figure 2. The picture of MEMS arrays: a. 1D MEMS arrays. b. 2D MEMS arrays.

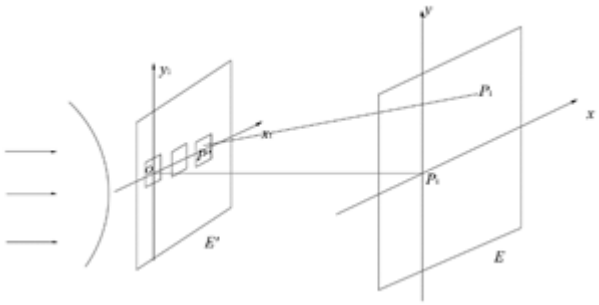

Figure 3. The schematize of Fraunhofer diffraction for 1D MEMS arrays.

3. Intensity Distribution Diffracted by 2-D MEMS Arrays

Supposing that a 2-D MEMS micro-mirror arrays are consist of $N\times N$ pieces of mirror, and Cartesian coordinate system is established as Fig. 4. On the basis of Kirchhoff diffraction theory, the complex amplitude of P_1 point in xP_0y plane is gotten as

Preprints (www.preprints.org) | NOT PEER-REVIEWED | Posted: 6 April 2021 doi:10.20944/preprints202104.0180.v1

$$\tilde{E}(x,y)=-\frac{ie^{ikz_1}}{\lambda z_1}e^{ik\frac{x^2+y^2}{2z_1}}A\sum_{h=0}^{N-1}\sum_{j=0}^{N-1}\int_{h(2a+d)-a}^{h(2a+d)+a}\int_{j(2b+d)-b}^{j(2b+d)+b}e^{-ik\frac{xx_1+yy_1}{z_1}}dx_1dy_1. \quad (13)$$

Similar to the principle of Eqs. (9) and (10), we get the following equation by integrating Eq. (13),

$$\tilde{E}(x,y)=4Cabe^{-i(N-1)\frac{\Delta_x+\Delta_y}{2}}\frac{\sin\beta}{\beta}\frac{\sin\alpha}{\alpha}\frac{\sin(N\Delta_x/2)}{\sin(\Delta_x/2)}\frac{\sin(N\Delta_y/2)}{\sin(\Delta_y/2)}, \quad (14)$$

where $\Delta_y=ky(2b+d)/z_1$. The optical intensity at P_1 point is obtained as

$$I(x,y)=|4Cab|^2\left(\frac{\sin\beta}{\beta}\right)^2\left(\frac{\sin\alpha}{\alpha}\right)^2\left(\frac{\sin(N\Delta_x/2)}{\sin(\Delta_x/2)}\right)^2\left(\frac{\sin(N\Delta_y/2)}{\sin(\Delta_y/2)}\right)^2. \quad (15)$$

Eq. (12) and Eq. (15) contain the common factor of $|4Cab|^2$, which is the optical intensity of the brightest spot in the observation plane when the laser is diffracted by a single mirror, for the convenience of calculating, it will be taken as a unit of optical intensity in the following paragraph. When the laser is diffracted by 1-D MEMS micro-mirror arrays, the optical intensity of the points in xP_0y plane is the minimum if their coordinates meet the equations of

$$\sin\alpha=0,\alpha\neq0 \quad \text{or} \quad \sin(N\Delta_x/2)=0,\sin(\Delta_x/2)\neq0, \quad (16)$$

namely,

$$\sin\alpha=0,\alpha\neq0 \quad \text{or} \quad \frac{x}{z_1}=\frac{\lambda n}{N(2a+d)},and\ \frac{n}{N}\neq m,(m,n=\pm1,\pm2\cdots) \quad (17)$$

For 2-D arrays, except for Eq. (17), other points in xP_0y plane are also located in dark spots if their coordinates meet the following equations,

$$\sin\beta=0,\beta\neq0, \quad \text{or} \quad \sin(N\Delta_y/2)=0,\sin(\Delta_y/2)\neq0, \quad (18)$$

namely

$$\frac{y}{z_1}=\frac{n\lambda}{2b}, \quad \text{or} \quad \frac{y}{z_1}=\frac{\lambda n}{N(2b+d)},\text{and}\ \frac{n}{N}\neq m,(m,n=\pm1,\pm2\cdots) \quad (19)$$

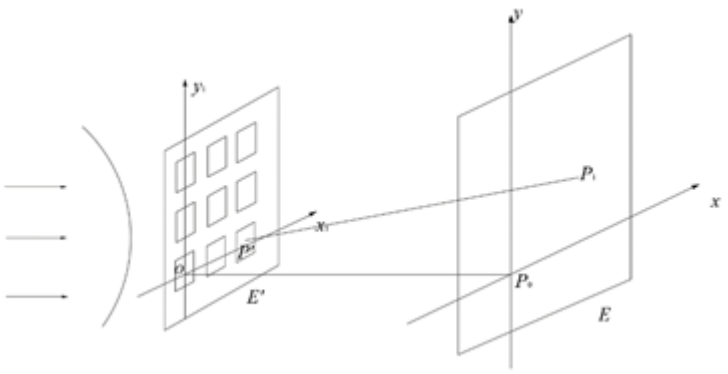

Figure 4. The schematize of Fraunhofer diffraction for 2D MEMS arrays.

Preprints (www.preprints.org) | NOT PEER-REVIEWED | Posted: 6 April 2021 doi:10.20944/preprints202104.0180.v1

Compared with dark spots, the maximum optical intensity location is rather difficult to locate. Although the location of the maximum optical intensity diffracted by 1-D and 2-D arrays can be derived from the derivative of Eqs. (12) and (15) in theoretical, their derivatives are so complicated that it is very difficult to get all roots of them in analytic expression. Furthermore, the exact coordinates of maximum optical intensity location is not as important as the detailed contrast of optical intensity in the observation plane, in other words, the specifics of intensity contrast is more important than the location of maximum intensity in the observation plane to design a Lidar based on MEMS arrays. Meanwhile the simulation of the intensity contrast is easier than calculating the derivatives of Eqs. (12) and (15).

4. Simulation of the Intensity

In this section, the distributions of optical intensity expressed by Eqs. (12) and (15) would be shown by simulation diagram, the rationality of Eqs. (12) and (15) is indirectly verified by comparing the simulation diagram with Young's double-slit experiment results. The mirror of either 1-D or 2-D arrays is 100 μm×100 μm, the pitch between two consecutive mirrors is 50 μm, (The parameters of MEMS are provided by Wio Tech Co.) the wavelength of laser is 1064 nm, and the distance from the plane of x_1Oy_1 to the plane of xP_0y is 20 m, in the other words, z_1=20 m. 1-D arrays and 2-D arrays are made up of 1×10 and 10×10 pieces of mirrors, respectively. Then the simulation figure of Eq. (13) as Fig. 5, while Fig. 6 is simulation of Eq. (15).

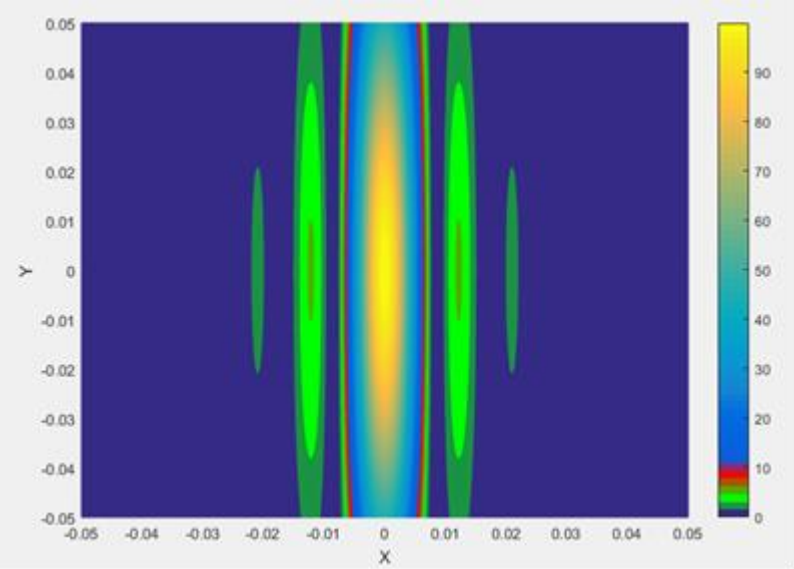

(a)

Preprints (www.preprints.org) | NOT PEER-REVIEWED | Posted: 6 April 2021 doi:10.20944/preprints202104.0180.v1

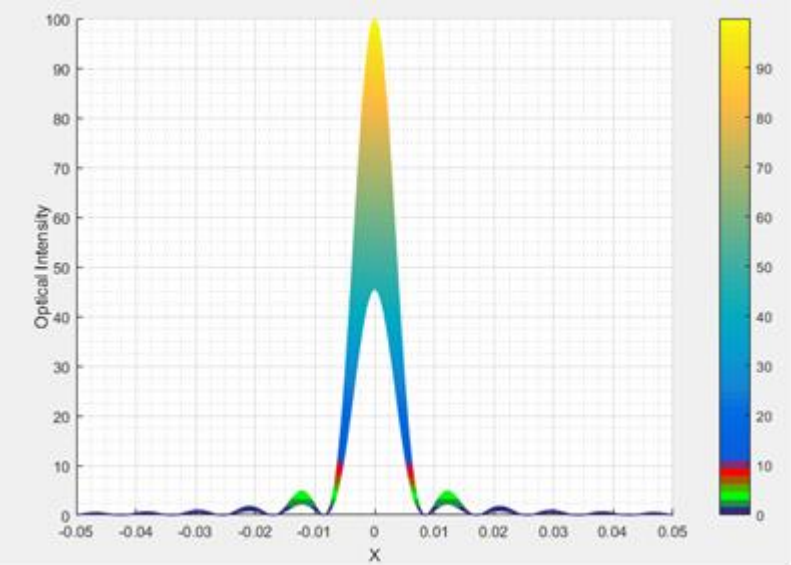

(b)

Figure 5. Diagram of optical intensity distribution diffracted by 1×10 arrays: (a). Streak distribution; (b). Intensity distribution.

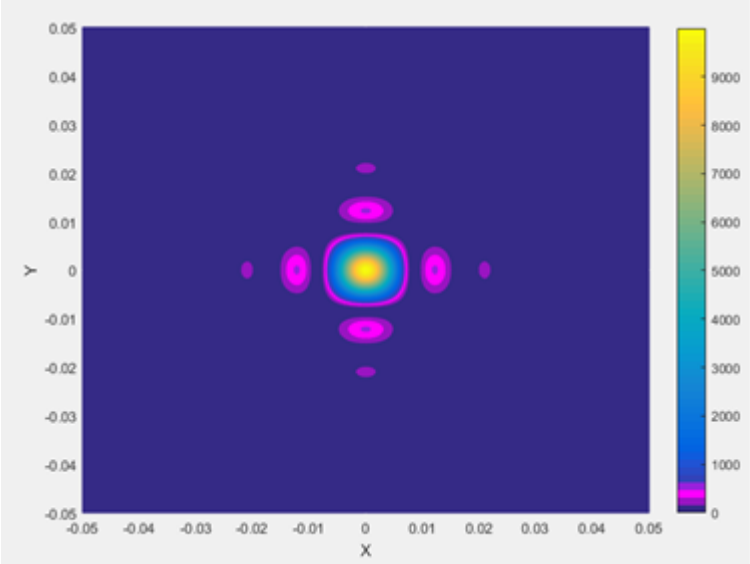

(a)

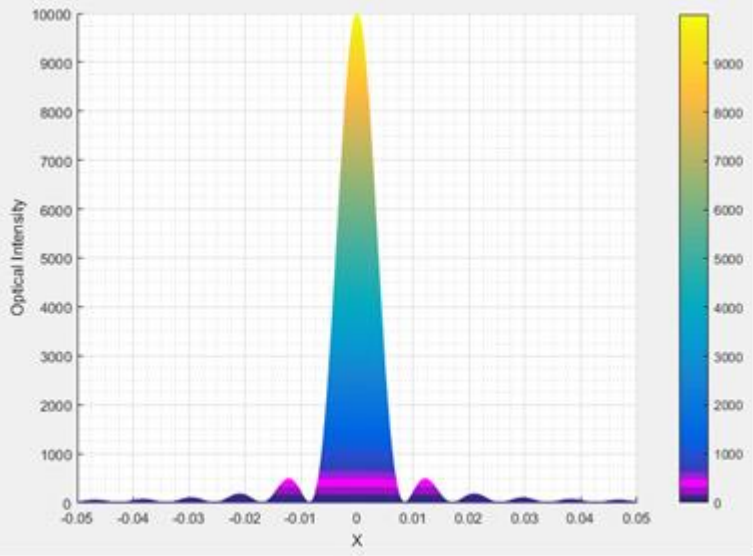

Preprints (www.preprints.org) | NOT PEER-REVIEWED | Posted: 6 April 2021 doi:10.20944/preprints202104.0180.v1

(b)

Figure 6. Diagram of optical internsity distribution diffracted by 10×10 arrays: (a). Spot distribution;(b). Intensity distribution.

In Fig. 6, it is obvious that the optical intensity of the brightest stripe is much greater than others, and the angular resolution of the maximum optical intensity spot is about 0.8 mrad. And this is fatal important for designing a scanning Lidar which is based on MEMS micro-mirror arrays.

We have customized some MEMS arrays, but as the limitation of engineering technology, the parameter and technology standard can't satisfy the theoretical requirements, so we can't directly prove the correctness of Eqs. (12) and (15). In order to prove the results are valid indirectly, we compare the results with Young's double-slit interference experiment. Although formulas (12) and (15) are obtained with the Fraunhofer diffracted condition (1), to some extent, we can get some valuable information of Eqs. (12) and (15) by comparing the simulation results of these equations with Young's double-slit interference experiment in the plane of 800 mm. Where the size of double slits is 0.02 mm×0.02 mm, the pitch between slits is 0.1 mm, and the wavelength λ is 1064 nm. Fig. 7 and 8 are double-slit interference simulating diagrams, and Fig. 9 is the diagram diffracted by 2×2 arrays.

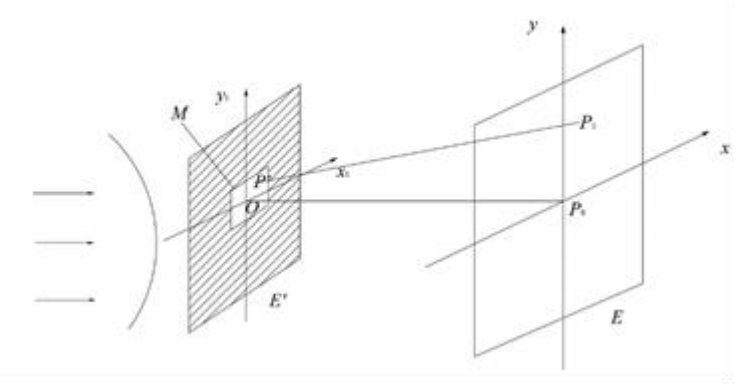

Figure 7. Streak distribution of Young's double-slit interference experiment.

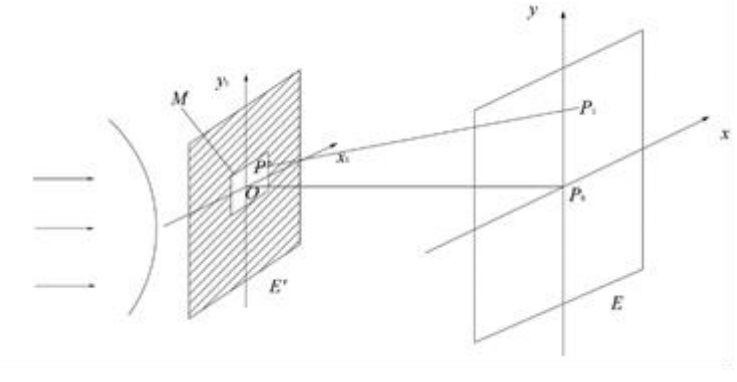

Figure 8. Spot distribution of Young's double-slit inference experiment.

Preprints (www.preprints.org) | NOT PEER-REVIEWED | Posted: 6 April 2021 doi:10.20944/preprints202104.0180.v1

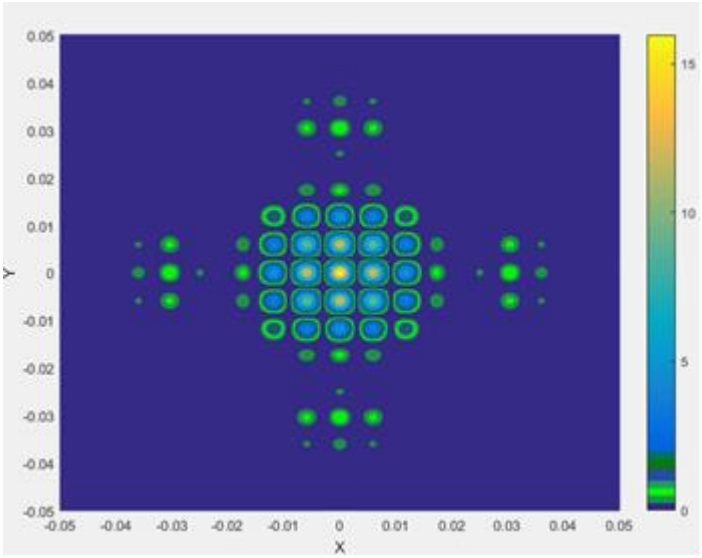

(a)

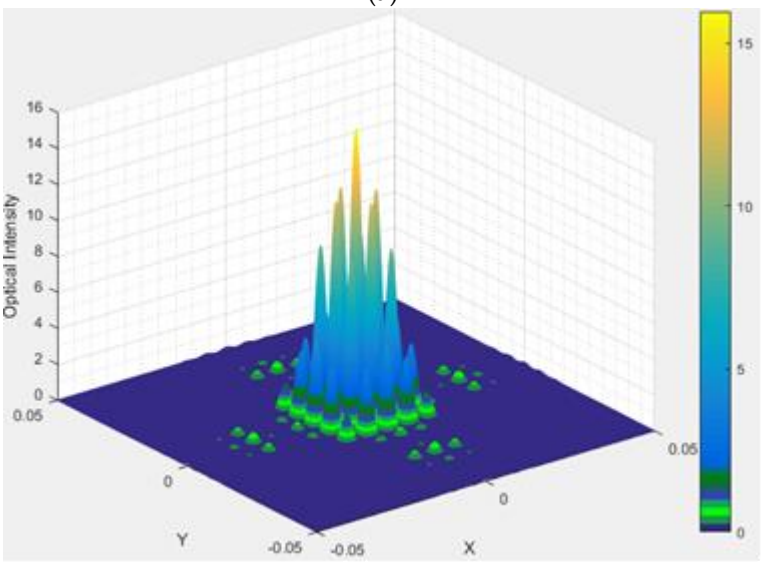

(b)

Figure 9. Spot and intensity distribution diffracted by 2×2 MEMS mirror arrays: (a). Plane figure of spot distribution;(b). Sterogram of intensity distribution.

From these figures, it is obvious that the contrast of optical intensity is low, and this corresponds to Young's double-slit experiment, in which the intensity of stripes is almost the same, while Eqs. (12) and (15) also show the number N of mirrors is determinant to optical intensity in observation plane. Besides, according to Young's theory, the pitch of stripes is

$$800\times1064\times10^{-3}\times10^{-9}\Big/\left(0.1\times10^{-3}\right)=0.0085\ \text{m} \tag{22}$$

The results of Fig. 7 is almost in accordance with Eq. (22), and this proves the results of Eqs. (12) and (15) are rationable.

5. conclusion

This paper is based on the Kirchhoff diffraction and Fraunhofer diffraction theory, the distribution functions of optical intensity are derivated when the laser is diffracted by 1-D and 2-D MEMS arrays, and we also provide the simulation results of the distribution. Also, we have indirectly proven the obtained results correctness by Young's double-split experiment. The conclusion, which the optical intensity of the greatest maximum stripe is much stronger than others, is very conspicuous, and the optical intensity in the observa-

tion plane would increase rapidly when the number of mirrors rises, so as the angle resolution of arrays. And the results in this paper reveal that using MEMS micro-mirror arrays to manipulate the laser beam can improve the resolution of Lidar comparing with using MEMS micro-mirror to realize it. Resolution is one of critical properties of Lidar, so the result we provided will give some references to assemble a laser scanning Lidar, especially for choosing laser radiation source and receiver sensor.

Acknowledgments: Thanks for National Natural Science Foundation of China (No. 62027283 and 61775048) and Shenzhen Fundamental Research Program (No. JCYJ2020109150808037) Funded.

Conflicts of Interest: The authors declare no conflict of interest.

1. Smith C.S. Piezoresistence effect in Germanium and Silicon. *Phys. Rev*. 1954, *94*, 42-49
2. Tufte O.N; Chapman P.W.; Long D. Silicon diffused-element piezoresistive diaphragms. J. Appl. Phys. 1962, *33*,3322-3327.
3. Courtney-Pratt J.S.; Mason W.P. Piezoresistive accelerometer. *US Patent 2963911*. Dec. 13, 1960.
4. Sanchez J.C. Semiconductor strain gauge. *US Patent 3084300*. Apr. 2, 1963.
5. Welkowitz W.; M. Traite. Piezoresistive transducer. *US Patent 3088323*. May 7, 1963.
6. Pfann W.G. Piezoresistive stress transducer. *US Patent 3186217*. June 1, 1965.
7. DeMichele D.J. Strain gauge pressure transducer. *US Patent 3350944*. Nov. 7, 1967.
8. Vick G.L. Strain gage configuration. *US Patent 3456226*. July 15, 1969.
9. Kotnik J.T.; Hamilton J.H. Pressure transmitter employing a diffused silicon sensor. IEEE Trans. Ind. Electron. Control Instrum. 1970, *IECI-17*,285-291.
10. Samaun, Wise K.D; Angell J.B. An IC piezoresistive pressure sensor for biomedical instrumentation. IEEE Trans. Biomed. Eng. 1973, *BME-20*,101-109.
11. Gayford M.L. Method for assembling electro-acoustical transducer diaphragm assemblies. *US Patent 3586792*. June 22, 1971.
12. Tsuge Y.; Koizumi N.; Vibration diaphragm and cone edge of a loudspeaker. *US Patent 3834486*. Sept. 10, 1974.
13. Garner A.V.; Townsend G.; Electro-acoustic transducer diaphragms. *US Patent 4020299*. Apr. 26, 1977.
14. Sugiyama S.; Suzuki T.; Kawahata K. et al. Micro-diaphragm pressure sensor. IEEE International Electron Devices Meeting. 1986,IEDM-86:184-188(Los Angeles, USA)
15. Ishihara T.; Suzuki K.; Suwazono S. et al. COMOS integrated silicon pressure sensor. IEEE J. Solid-State Circuit, 1987, *22*,151-156
16. Roessig T.A.; Howe R.T.; Pisano A.P. et al. Surface-micromachined resonant accelerometer. IEEE Proceeding of International Solid State Sensors and Actuators Conference. 1997(Chicago, USA)
17. Fujii T.; Kuroyanagi S.; Gotoh Y. Semiconductor sensor for accelerometer. *US Patent 5313836*. May 24, 1994
18. Weigold J.W.; Brosnihan T.J.; Bergeron J. et al. A MEMS condenser microphone for consumer application. IEEE International Conference on Micro Electro Mechanical System. 2006 (Istanbul, Turkey)
19. Bogue R. Recent developments in MEMS sensors: a review of applications, markets and technologies. *Sensor Review*, 2013, *33*,300-304
20. Motamedi M.E. MOEMS: Micro-Opto-Electro-Mechanical System. SPIE Press: Washington. 2005
21. Li H.G. Micro-opto-electro-mechanical systems technologies and applications. Transducer and Microsystem Technologies. 2011, *30*,1-3(in Chinese)
22. Riza N.A.; Ghauri F.N. Super resolution hybrid analog-digital optical beam profiler using digital micromirror device. IEEE Photonics Technol. Lett. 2005, *17*,1492-1494
23. P. B. Ruffin. Optical MEMS-based arrays. Proceeding of SPIE- Smart Structure and Materials. 2003, 5055:230-241
24. Cai D.; Yao J.; Jiang W. Optical efficiency of MEMS deformable mirror for adaptive optics. Proceeding of SPIE, MEMS Adaptive Optics III. 2009, *7209*,72090Q
25. Brunne J.; Wallrabe U. Tunable MEMS axicon mirror arrays. Opt. Lett. 2013, *38*,1939-1941.
26. Luo S.; Wang D.; Tang J.; L. Zhou et al. Circumferential-scanning endoscopic optical coherence tomography probe based on a circular array of six 2-axis MEMS mirror. Biomed. Opt Express, 2018, *9*,2104-2114.